Semiconducting Single-Walled Carbon Nanotubes on Demand by Polymer Wrapping

*Widianta Gomulya, Guadalupe Diaz Costanzo, Elton J. Figueiredo de Carvalho, Satria Zulkarnaen Bisri, Vladimir Derenskyi, Martin Fritsch, Nils Fröhlich, Sybille Allard, Pavlo Gordiichuk, Andreas Herrmann, Siewert Jan Marrink, Maria Cristina dos Santos, Ulrich Scherf, and Maria Antonietta Loi**

Single-walled carbon nanotubes (SWCNTs) are one of the most interesting components of the large family of the carbon materials. After more than 25 years from the discovery of its first nano-member, the buckyball, carbon-based materials continue to fascinate scientists and engineers with their properties and the continuous findings of new members.[1] Many of the exciting properties of the one-dimensional member of the family, carbon nanotube, stem from the strong relation between size, structure, and electronic properties. Nevertheless, these properties also lead to highly polydispersed (in term of diameter, helicity and length) samples that so far have limited carbon nanotubes applicability in technology. In fact, although synthetic procedures have been largely improved in the last years, none of the many methods available is able to provide a homogeneous and narrow population of carbon nanotubes.

Recently, the awareness of these limitations has caused a change of paradigm in the literature. For years, scientists concentrated their attention on demonstrating the many properties of carbon nanotubes by fabricating highly performing field-effect transistors, light-emitting devices, logic gates, interconnects, sensors, and nano-mechanical devices.[2–6] In the last few years, greater efforts have been devoted to the development of sorting techniques by which specific populations of carbon nanotubes can be separated and effectively used in large scale.[7,8]

The non-covalent functionalization of SWCNTs is widely investigated due to its advantages over other techniques, especially the fact that it leaves the sidewalls relatively unaffected and consequently, the physical properties of the nanotubes remain nearly unchanged. Using strategies borrowed from biochemistry and life science such as the encapsulation of SWCNTs with surfactants followed by density gradient ultracentrifugation[8–10] and encapsulation with DNA with specific sequences,[11] important results in separating metallic from semiconducting nanotubes were obtained. Recently, unprecedented chirality selection in large scale has been achieved by using gel chromatography (single-surfactant what time is toda gel chromatography).[12] However, of all these water-based methodologies only the last appears to be promising for industrial scale-up.

Very efficient helicity discrimination was obtained in the past few years by using the spontaneous wrapping of conjugated polymers such as the fluorene-based homo- and co-polymers around SWCNTs of about 1 nm diameter, synthesized by chemical vapor deposition with cobalt and molybdenum oxide as catalyst (CoMoCAT) or by high-pressure carbon monoxide (HiPco).[13] These are self-assembled hybrid structures where the polymer chain is wrapped around the SWCNTs, and the side chains of the polymer allow solubilization of the hybrid in common organic solvents. From the first report, many different polymer structures[14–20] have been tested with the aim of finding the ones that are able to discriminate SWCNTs of different diameter and helicity on demand. However, all the polymers tested, including the most efficient poly(9,9-dioctylfluorene-2,7-diyl) (PFO; here called PF8), have been demonstrated to be effective only with small (0.8-1.2 nm) diameter tubes. Initially, it was believed that the discrimination mechanism had to be ascribed mainly to the nature of the polymer backbone. Recent studies gave indications that also the side chains of the polymer have an important role in the wrapping and selection mechanism.[17,21]

Here we demonstrate the selection of semiconducting SWCNTs in a wide diameter range (0.8-1.6 nm) using polyfluorene-derivatives with alkyl chains of increased length. By leaving the backbone of the polymer unchanged we find that SWCNTs of different diameters can be selected by tuning the length of the alkyl side chains of the polymer. Semiconducting SWCNT of diameters larger than 1.2 nm, for which post-synthetic separation methodologies did not exist to

W. Gomulya, G. D. Costanzo, E. J. F. de Carvalho, Dr. S. Z. Bisri, V. Derenskyi, P. Gordiichuk, Prof. A. Herrmann, Prof. S. J. Marrink, Prof. M. A. Loi
Zernike Institute for Advanced Materials
University of Groningen
Nijenborgh 4, Groningen 9747 AG, The Netherlands
E-mail: M.A.Loi@rug.nl
G. D. Costanzo
Physics Department
Faculty of Sciences
University of Buenos Aires
Ciudad Universitaria
C1428EGA, Buenos Aires, Argentina
E. J. F. de Carvalho, Prof. M. C. dos Santos
Instituto de Física
Universidade de São Paulo
05508-090 São Paulo SP, Brazil
M. Fritsch, N. Fröhlich, Dr. S. Allard, Prof. U. Scherf
Chemistry Department and Institute for Polymer Technology
Wuppertal University
Gauss-Str. 20, D-42119 Wuppertal, Germany

DOI: 10.1002/adma.201300267

© 2013 WILEY-VCH Verlag GmbH & Co. KGaA, Weinheim

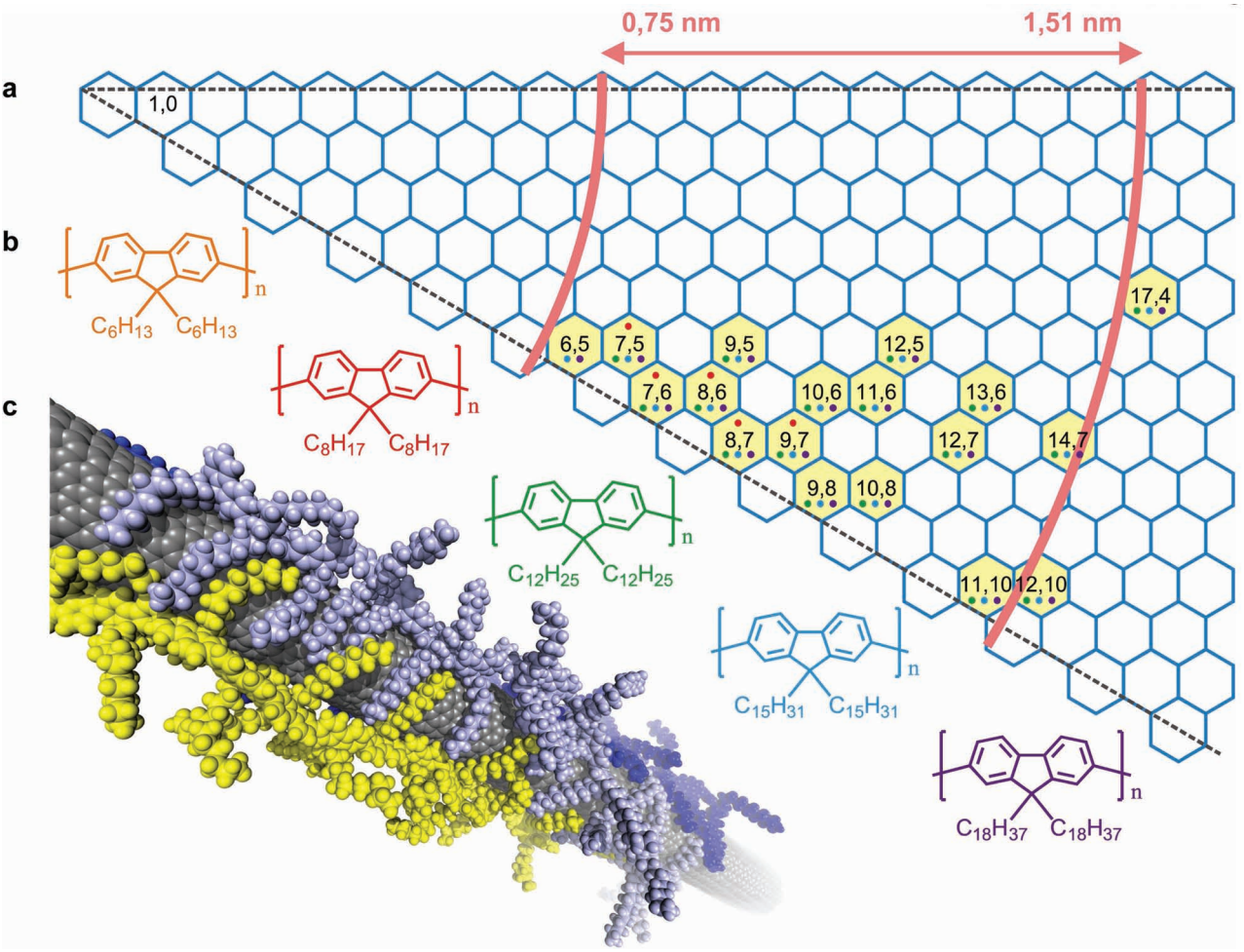

Figure 1. (a) Chirality map of SWCNTs selected by polymer wrapping. In yellow the SWNTs selected are underlined; the color of the dots inside the hexagons indicates which of the polyfluorene derivatives (color code used for the chemical structures) is able to select the nanotubes. (b) Chemical structure of the polyfluorene derivatives used: PF6, PF8 (commonly known as PFO), PF12, PF15, and PF18. (c) Structure as obtained by molecular dynamics simulations of three PF12 chains wrapped around a (12,10) nanotube after 10 ns at constant-pressure in toluene solution.

date, can now be efficiently selected. The high concentration, extremely important for application, of semiconducting SWCNTs is demonstrated by optical spectroscopy and by fabrication of highly performing network field-effect transistors with mobilities up to 14 $cm^2\ V^{-1}\ s^{-1}$ for holes and 16 $cm^2\ V^{-1}\ s^{-1}$ for electrons, and on/off ratio of 10^5. The role of the alkyl chain length in the sorting of semiconducting SWCNTs is rationalized by means of molecular dynamics simulations.

Two different commercially available sources of SWCNTs, HiPco (diameter between 0.8–1.2 nm) and arc plasma jet (SO) (diameter of about 1.4 nm), were dispersed in toluene using polyfluorene derivatives bearing alkyl side chains of length ranging from C_6H_{13} up to $C_{18}H_{37}$. The chemical structures of the 5 polymers used are shown in **Figure 1**b. The dispersion was prepared following a similar recipe to the one reported by Nish et al.[13] for polyfluorene (PF8)-based dispersions. Cuphorn sonication was performed for about 2 h to debundle the SWCNTs. The suspension was then immediately centrifuged for 2 h. Finally, the supernatant portion was extracted and used for optical investigations.

Figure 1a shows the chirality map of the SWCNT solution as derived from the optical measurements. In this map, the yellow hexagons indicate the species of SWCNTs that are successfully selected. The colors of the dots inside the yellow hexagons show which of the 5 polymers, according to the color code of Figure 1b, are able to select the specific tubes. Figure 1c displays a snapshot of the molecular dynamics (MD) simulation showing 3 polymer chains wrapped around a (12,10) carbon nanotube in presence of toluene.

The chirality map shown in Figure 1a results from the analysis of the absorption spectra of the HiPco and SO samples are reported in **Figure 2**a and 2b. The absorption peaks were assigned to specific tubes by using the empirical formula[22]:

$$E_{11} = \frac{1241}{A_1 + A_2 d} + A_3 \frac{\cos 3\theta}{d^2} \quad (1)$$

In Equation 1, E_{11} is the energy of the first electronic transition of a (n,m) semiconducting nanotube which its chiral angle and diameter are θ and d, respectively. The constants A_1, A_2 and A_3 were adjusted to account for the spectroscopic data of

© 2013 WILEY-VCH Verlag GmbH & Co. KGaA, Weinheim

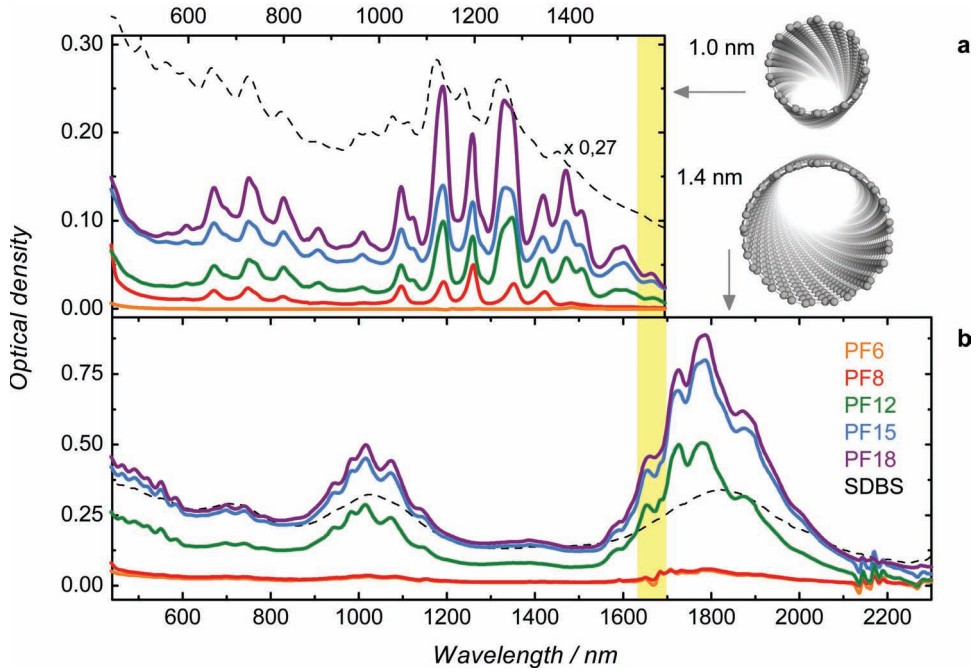

Figure 2. (a) Absorption spectra of HiPco SWCNTs (average diameter 1 nm) dispersed with different derivatives of polyfluorene in toluene (continuous lines,with the color code for the different polymers is given in the panel (b)) and dispersed with SDBS in water (dashed line). (b) Absorption spectra of SO SWCNTs (average diameter 1.4 nm) dispersed with different polyfluorene derivatives in toluene (continuous lines, with color codes indicated in the legend) and dispersed with SDBS in water (dashed line).

SWCNTs suspended in toluene solutions of PF8.[21] The fitted constants are $A_1 = 174.3$ nm, $A_2 = 1083.0$, $A_3 = 0.020$ eV·nm^2 ($j = 2$) or $A_3 = -0.065$ eV·nm^2 ($j = 1$), where $j = \text{mod}(n\text{-}m,3)$.

Figure 2a shows the spectra of the HiPco SWCNTs selected using the 5 different polyfluorene-based polymers. The dispersions show an increasing optical density (OD) in going from shorter alkyl chain (PF8) to the longer ones. In the plot, the spectrum of the unsorted HiPco SWCNTs (obtained with sodium dodecylbenzene sulphonate (SDBS) in D_2O) is shifted in the *y*-direction and shown for comparison. A clear correlation, evident from the absorbance spectra, exists between the lengths of the polymer side chain and both the quantity and the type of sorted SWCNTs. For instance, PF6 is unable to wrap SWCNTs and PF8 specifically selects five different semiconducting species.[13,21] The dispersions obtained with the three polymers with longer alkyl chains, namely PF12, PF15, and PF18, show a higher density of SWCNTs (higher OD); and, at the same time a larger number of semiconducting SWCNTs species of larger diameter (the ones appearing with absorption peaks around 1400 nm). The extra species that can be selected with PF12, PF15, and PF18 with respect to PF8 are: (11,9); (10,2); (9,5); (10,6); (9,8); (10,8); (12,5); (10,9), etc.

To check the capability of PF12, PF15, and PF18 polymers to select large diameters carbon nanotubes, the experiments were repeated using SO SWCNTs, which have an average diameter of about 1.4 nm. The absorption spectra of SO SWCNTs dispersed with the different derivatives of polyfluorenes are shown in Figure 2b. The dashed black line represents the absorption spectrum of the SO SWCNTs dispersion obtained with SDBS. For this class of large diameter SWCNTs, the individualization with SDBS is the only method available to date. Differently from HiPCO tubes, for these large diameter SWCNTs, neither PF6 nor PF8 could select any nanotube species. However, SO SWCNTs are efficiently sorted when dispersed with PF12, PF15, and PF18. This observation confirms the trend evidenced for HiPco tubes of selecting more and larger SWCNTs with polymers with the longer side chains. It is evident that the long alkyl chain polymers PF12, PF15, and PF18 have not only a preference for larger tubes, but also do allow selecting an extremely broad distribution of SWCNTs species with bandgaps from 950 nm (1.3 eV) to almost 2000 nm (0.6 eV). The yellow band in Figure 2 indicates the (10,9) SWCNT that is present in both HiPco and SO samples as evidence for the fact that the polymers are discriminating the kind of nanotubes independently from the amount of starting species.

Until recently, the effective separation and selection of large diameter tubes (>1.2 nm) has never been achieved, neither with density gradient centrifugation, nor with any of the noncovalent functionalization of the SWCNTs sidewalls. Tange et al.[15] has reported the extraction of the (15,4) nanotube from an SO SWCNT sample; but with low efficiency of the extraction process, indicated from a very small value of the absorbance of their sample in the E_{22} transition (lower than 0.01). The result displayed in Figure 2b demonstrated almost 100-times more efficient extraction of the large diameter tubes than any other reported methods.

To shine light on the selection mechanism for large diameter tubes, we investigated the interaction of polyfluorenes chains with such nanotubes through classical molecular dynamic simulations. Impulse Dynamics was used to allow the polymer

© 2013 WILEY-VCH Verlag GmbH & Co. KGaA, Weinheim

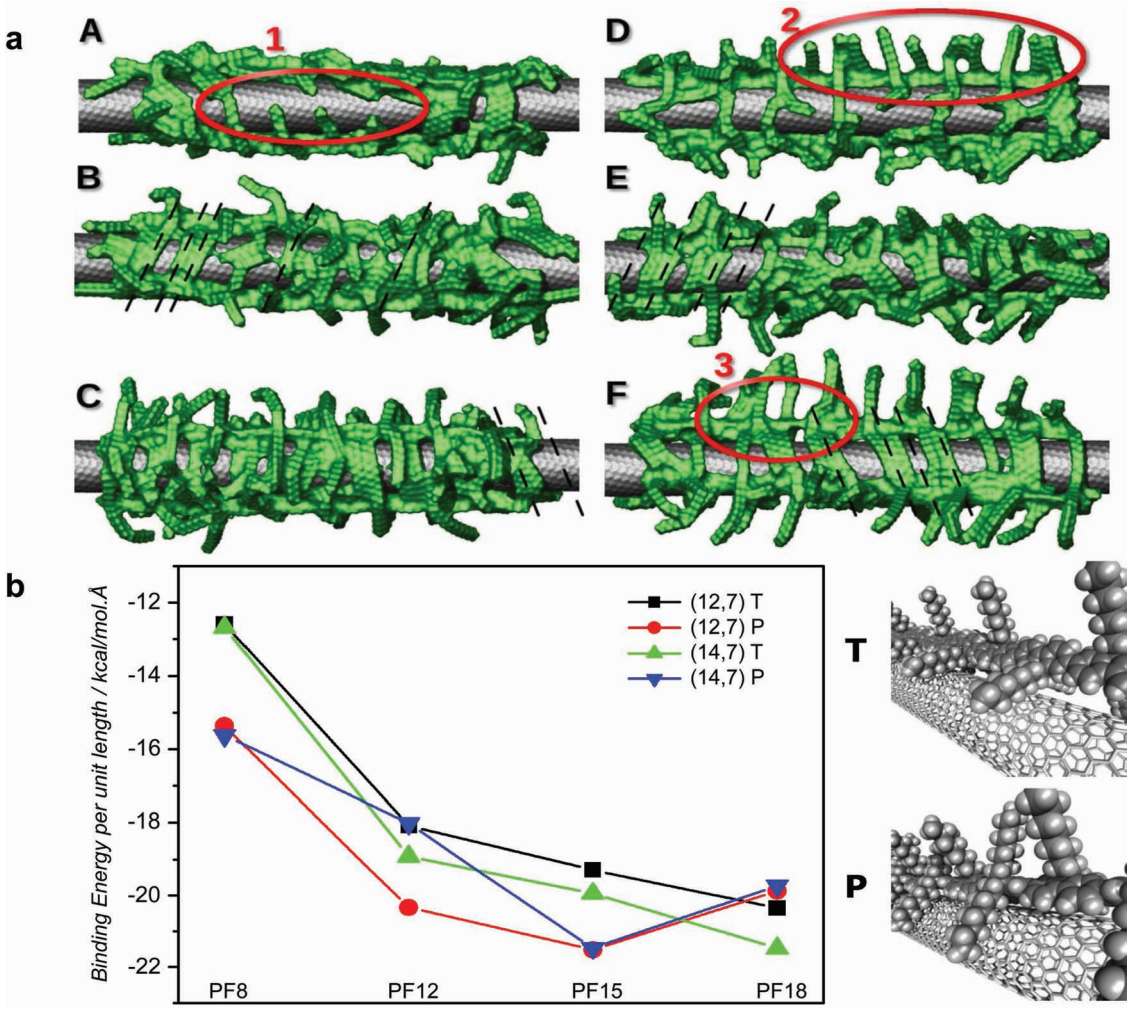

Figure 3. (a) Molecular models of the optimized structures of (14,7) nanotube covered by three polymer chains in the T (left) and P (right) configurations. From top to bottom: PF12, PF15, and PF18. The red circles indicate: (1) uncovered nanotube surface; (2) alkyl tails oriented outward the nanotube surface; (3) detaching of polymer backbone from nanotube wall. (b) Binding energy divided by the length of the nanotube covered by the polymers. On the right side of the figure are shown the configurations with the polymer backbone perpendicular (T) and parallel (P) to the tube surface.

chain to adopt an initial directional velocity toward the nanotube. We focused on the tubes (14,7) and (12,10), which correspond to the highest absorption in Figure 2b, as well as (12,7) and (10,9). These pairs of tubes have similar absorption energies and diameters, but different chiralities. While most of the absorption peaks of the SO SWCNTs sample can be assigned to nanotubes close to the armchair geometry, the contribution from the other chiralities should not be discarded. Interestingly, the other tubes selected near the armchair have chiral angles close to 20°. PF8 is known to wrap on the near armchair nanotubes, adopting a helical conformation due to the ordered β-phase in toluene solutions.[21] Polyfluorenes having longer pendant groups do not present a β-phase and can assemble in different geometries on the tubes.[23] We considered the following possibilities: the polymer can attach to the nanotube with the long molecular axis along the nanotube axis or form a helix; and the aromatic backbone can be parallel to the tube surface as in a π-stacking (P-configuration), or can be perpendicular to the tube (T-configuration) thus exposing the pendant groups to the surface.

Figure 3a illustrates the resulting geometries on tube (14,7). The polymer chains do not spontaneously adopt a helical conformation on this tube, as they tend to do in near armchair tubes. This figure shows the solvent-accessible surface calculated by the Connolly algorithm[24] and by using a probe radius consistent with toluene. Structures to the left are in T geometry and those to the right are in the P geometry.

In going from PF12 to PF18, corresponding to the labels A, B, and C in T geometry, and D, E, and F in P geometry, we saw the increase of the nanotube area covered by the polymer chains. The red circle (1) in structure A points to the considerably large surface of the nanotube that remains uncovered. Another chain can attach this region, but it would not be strongly attached since the area is not large enough. We noticed during the simulations that the chains tend to cluster together and allow the inter-digitation of the alkyl groups. The dashed lines on B and

© 2013 WILEY-VCH Verlag GmbH & Co. KGaA, Weinheim

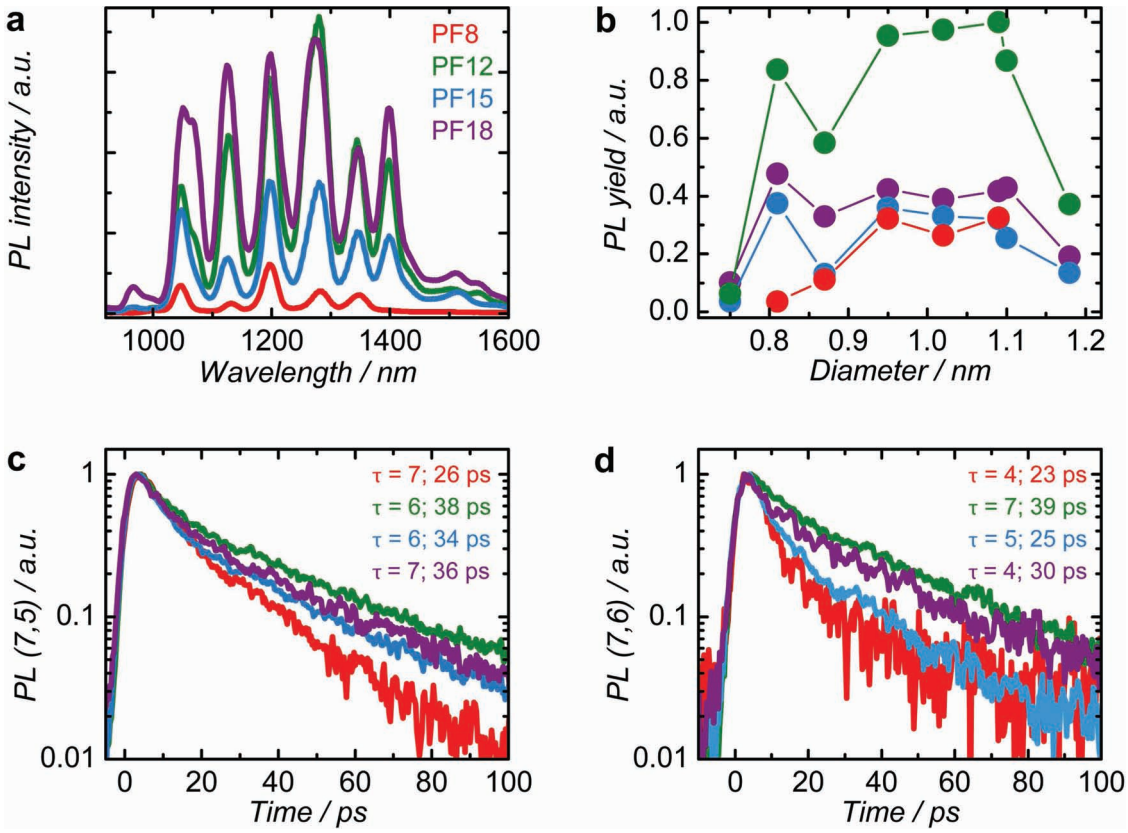

Figure 4. (a) Photoluminescence intensity of HiPco SWCNTs wrapped with different polyfluorene derivatives. (b) Photoluminescence yield of different SWCNTs wrapped by polyfluorene derivatives. (c) Decay of the photoluminescence of (7,5) tubes wrapped by different polyfluorene derivatives. (d) Decay of the photoluminescence of (7,6) tubes wrapped by different polyfluorene derivatives.

E show that the alkyl groups tend to align on the network of bonds following the tube chirality. It is also apparent that the T configuration provides a better coverage of the tube surface. The circle in D (2) highlights the number of lateral chains pointing outwards in P configuration and thus not contributing to the polymer binding. Finally, the circle (3) in F shows that the polymer in P configuration is sometimes detached. It is a feature that was not observed in near armchair tubes.

The binding energies, defined as the difference between the energy of hybrid structure and the sum of energies of its isolated parts, were calculated for the final geometries and divided by the length of the covered surface. The results are shown in Figure 3b for tubes (12,7) and (14,7), together with an illustration of the T and P geometries. Given that the conjugated backbone is the same, this figure evidences the important role played by the lateral chain. The binding energy increases as the lateral chain increases. Although PF12 gives a better binding in the P geometry (the π–π interaction compensates the worse surface coverage compared to the T geometry), the binding energies tend to be independent of the backbone configuration when the lateral chain is long enough. A similar behavior was found in near armchair nanotubes as well: for instance, the binding energy for (12,10) nanotube wrapped by PF12 is –18.0 kcal mol^{-1} Å^{-1} in P geometry and –16.0 kcal mol^{-1} Å^{-1} in T geometry; the difference is the tendency of the polymer to form a helix. The following conclusions can be drawn from the molecular modeling: (i) nanotube walls are better covered by the polymers when the alkyl chains are longer, which prevents re-bundling of nanotubes; (ii) the selectivity decreases as the alkyl chain increases since the polymer wrapping can adopt more configurations; (iii) the van der Waals interaction between alkyl chains and nanotube walls dominate the wrapping process when the lateral chains are long enough.

The photoluminescence spectra of the HiPco samples obtained with the different polyfluorenes confirm the high quality of the dispersions and the ability of the long alkyl chain polymers to select SWCNTs with emission above 1400 nm, such as (9,8); (10,8); (12,5); and (10,6) that could not be sorted with PF8 (**Figure 4**a). Individualized SWCNTs are expected to have higher quantum yields than bundles; in the latter case, there is a higher chance of quenching due to migration of the photoexcitation. Consequently, the photoluminescence yield is one of the most sensitive measurements for assessing the quality of SWCNT dispersions. An estimation of the photoluminescence yield (Figure 4b) of the PF-wrapped SWCNTs is obtained by normalizing the photoluminescence intensity measured for each carbon nanotube (as shown in Figure 4a) for their absorbance (reported in Figure 2a). Besides for the (11,9) tube, all the other tubes are better individualized by PF12, with almost twice higher PL yield with respect to what is obtained with the other polymers. A further evidence of the highest quality of the PF12-based dispersion is provided by the lifetime of the photo-

© 2013 WILEY-VCH Verlag GmbH & Co. KGaA, Weinheim

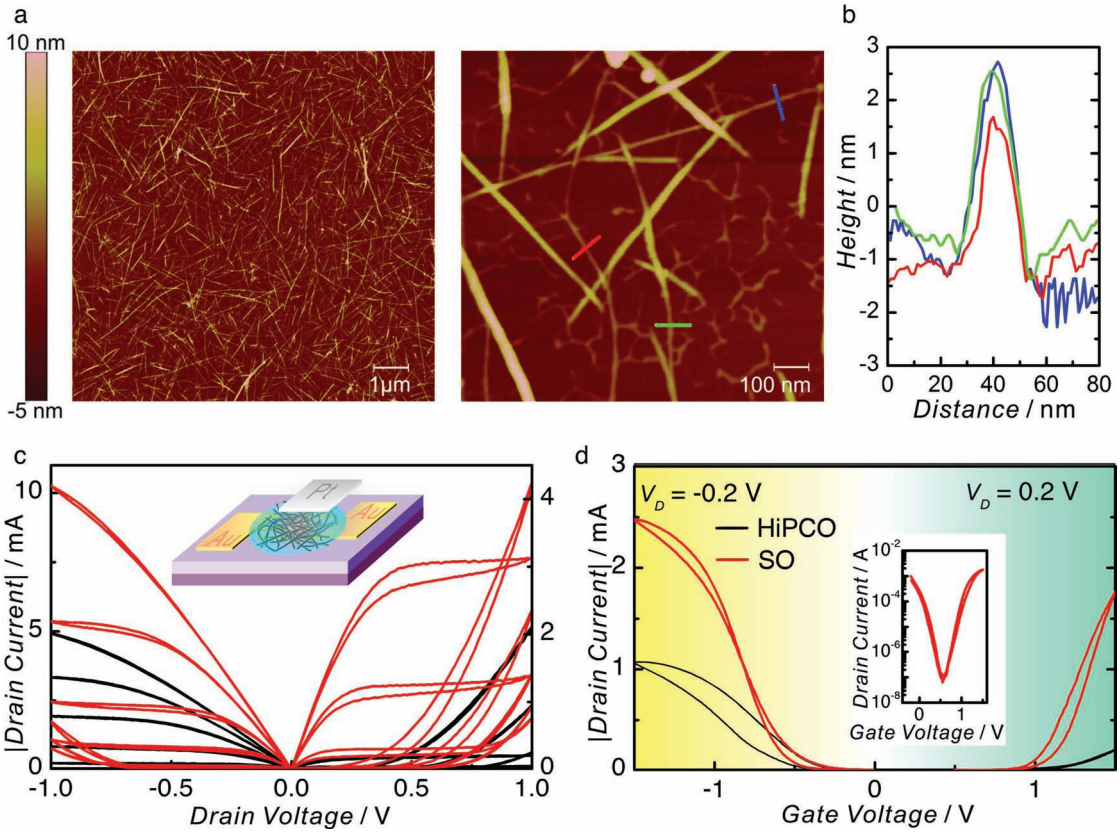

Figure 5. (a) Atomic force microscopy (AFM) images of a randomly distributed SO SWCNT network on a mica substrate. (b) Height profile of three different SWCNTs from the AFM image showing an average diameter of about 3 nm. (c) I_D-V_D output characteristics of ion-gel gated transistors (inset) made from HiPCO SWCNTs (black curves) and SO SWCNTs (red curves). (d) The comparison of the I_D-V_G transfer characteristics of the corresponding devices for both p-channel and n-channel operations. The inset shows the logarithmic scale plot of the transfer curve of the transistor (V_D = 0.2 V) made from SO SWCNTs, from which on/off ratio >10^4 for electron is obtained.

luminescence of the SWCNTs. In Figure 4c and 4d, the decays for the (7,5) and (7,6) tubes are reported, respectively. For both SWCNTs, the longer lifetime values (τ_1 = 6 ps; τ_2 = 38 ps) were recorded from the PF12-wrapped tubes.

By using long side chain polymers, we succeeded to obtain dense dispersions with absorbance more than one order of magnitude higher than any other reported techniques.[17] By using this highly concentrated dispersion of SO SWCNTs, dense networks of tubes on a substrate were prepared. AFM pictures of these networks are displayed in **Figure 5**a. Interestingly, the average length of the nanotubes in the images is larger than 1.5 μm, which is superior to 1/3 of their original length. Sonication is often considered causing damage on the nanotubes and reducing their length.[7] However, our results suggest the SO tubes retained a large part of their total length. From these AFM images, the average diameter of the SWCNTs wrapped by the polymers was estimated to be about 3 nm (see Figure 5b). According to our MD simulations, the hybrid formed by the (12,10) nanotube covered by four PF12 chains in the T configuration, in which most of the alkyl chains are wrapped around the tube surface, has an average diameter around 2.8 nm, without taking account the atomic van der Waals radius. This MD result is consistent with the experimentally-measured diameter and shows that the tubes are covered with a single polymer layer.

Sorting SWCNTs of large diameter has enormous relevance for the fabrication of highly performing SWCNTs-based field-effect transistors and for all the applications in the telecommunication-window wavelengths (C-band = 1.53–1.57 μm). In large-diameter nanotubes, carrier scattering processes are reduced. Scattering due to defects is attenuated because of the dilution of the defect influence on the carrier wavefunctions. Moreover, the radial breathing mode (RBM) phonon energy is inversely proportional to the tube diameter; and for tubes in the diameter range of 1.5–2.0 nm, its RBM phonon energy is comparable to the thermal energy at room temperature. Consequently, large-diameter SWCNTs are the best choice for electronic applications because of the reduced electron (and hole) scattering with the phonon modes.[2]

To demonstrate the effectiveness of the nanotube sorting and purification using the long side-chain polyfluorenes, we used PF12 wrapped HiPco SWCNT and the SO SWCNT as active materials for field-effect transistors. We fabricated the transistors following previously reported procedures,[25] in which the random network of nanotubes was deposited using a simple drop casting method, followed by high temperature

© 2013 WILEY-VCH Verlag GmbH & Co. KGaA, Weinheim

annealing to remove the polymer. Both HiPco and SO SWCNTs transistors were prepared from enriched solutions with similar initial concentration of nanotubes. SDBS-dispersed SWCNTs based transistors are not reported because of their metallic behavior.

In addition to conventional SiO_2 dielectric, ion gel of 1-ethyl-3-methylimidazolium bis(trifluoromethylsulfonyl)imide ([EMIM][TFSI]),[26] was utilized to create electric-double-layer (EDL) gated transistors (inset Figure 5c). The ion-gel gating allows induction of a very high carrier density accumulation ($n \sim 10^{14}$ cm^{-2}) with a very low driving voltage ($V_D, V_G < 1.5$ V). Because of the high carrier density, which will bring the device in a regime where trap states are filled, this type of gating allows observing the intrinsic characteristics of the semiconductor under study.[27]

Figure 5c compares the I_D-V_D output characteristics of the ion-gel gated FETs of HiPCO and SO nanotubes. The devices were driven with small voltages, up to 1.0 V of V_D and up to 1.5 V of V_G, which was well within the electrochemical window of the ion gel. Both type of the devices exhibit high performance ambipolar characteristics, in which clear linear and saturation behaviors were observed for both hole and electron accumulations. The linear regime of both hole and electron demonstrated ohmic behavior, despite the band mismatch of the Au electrode and the SWCNTs LUMO level tends to induce Schottky-type injection barrier (particularly) for electrons.[25] This behavior can be attributed to the enhancement induced by the ion gel of the electric fields at the interface between Au and the SWCNTs.[28] Both the HiPCO and the SO SWCNT devices exhibited high on/off ratios (exceeding more than 10^4 and 10^5 at $V_D = 0.2$ V). A very steep sub-threshold swing (SS) of 70 mV·dec^{-1} is observed for hole accumulation in the SO SWCNT FET. Values slightly larger for the electron accumulation 110 mV·dec^{-1} are observed. For the HiPco SWCNT FET, the SS was 100 mV·dec^{-1} and 90 mV·dec^{-1} for holes and electron, respectively. The values in both devices are very small and close to the ultimate limit ($SS = 66$ mV·dec^{-1}), which can only be achieved in an ideal transistor device with negligible charge traps operated at room temperature.[29] These findings indicate a remarkable coupling between the ion-gel gate and the SWCNT film of both HiPco and SO tubes, with virtually no significant charge trapping.

To quantify the high performance of the SWCNT transistors, the mobility values of both holes and electrons are extracted from their I_D-V_G characteristics (Figure 5d). We obtained the effective charge carrier mobilities using the equation $\mu = (L_C/W_C)(eV_D)^{-1}(dI_D/dn)$ in the linear region, where L_c and W_c are the device channel length and width, respectively; e is the elementary charge; and n is the V_G-dependent charge carrier density accumulated by the ion-gel gate. The value of n is estimated using the equation $n = (1/e)\int C_i dV_G$ in which C_i is the V_G-dependent capacitance value of the ion-gel gate. The measured $C_i(V_G)$ are in the order of μF·cm^{-2} at V_G values within the electrochemical window (C_i(-1 V) = 3.4 μF·cm^2; and C_i(1 V) = 3.0 μF·cm^2). As a consequence, the maximum value of charge carrier accumulation is as high as 2.5×10^{13} cm^{-2}.

We obtain hole and electron mobilities of about 5.7 cm^2 V^{-1} s^{-1} and 3.6 cm^2 V^{-1} s^{-1}, respectively, for HiPco SWCNT FET. For SO SWCNT FET, even higher hole (14.3 cm^2 V^{-1} s^{-1}) and electron (16.4 cm^2 V^{-1} s^{-1}) mobilities are achieved. These mobilities are extremely high especially considering that the network we were fabricating was relatively sparse. Since the purification of both nanotube sources was done with similar amount of starting material, the results of device performance show that the larger diameter SO tubes yielded higher performance than the smaller diameter HiPco tubes. Generally, the length of the tubes is considered to be a limiting factor for the achievement of high field effect mobility, in our case the HiPco tubes after treatment have an average length of 2 ± 1 μm, that is slightly longer than the average length of the SO tubes (1.5 μm). It should be noted that the quantum capacitance of carbon nanotube (0.8 pF·cm^{-1})[30] is far smaller than the measured capacitance of the ion-gel gate and its influence dominates in sparse coverage of the tube on the channel, as in the prepared transistors. As consequence, the effective mobility values will be much larger than those estimated above. Nevertheless, the combination of high carrier mobilities, high on/off ratios and minimum traps proved the effectiveness of the SWCNT separation of both small and large diameter tubes using this method.

In conclusion we have demonstrated that large diameter semiconducting carbon nanotubes can be efficiently separated and individualized using long alkyl chain polyfluorene derivatives. These polymers exhibit affinity for a number of semiconducting SWCNT chiralities contained both in small diameter nanotubes (diameter between 0.8-1.2 nm) as well as in large diameter tubes (diameter of about 1.4 nm). In both cases, polyfluorenes with long side chains allow obtaining dispersions of highly individualized semiconducting SWCNT with very high concentration and contain SWCNT species that could not be selected previously. The understanding of the wrapping process is provided by molecular dynamics simulations, which showed that the long alkyl tails on polyfluorenes provide a stronger binding to the nanotube wall and a variety of wrapping geometries that allow more nanotube species to be suspended. These results are consistent with a more efficient solubilization and a less specific selection of nanotube chiralities as the length of the alkyl chains increases, as observed experimentally.

The high quality of the sample, in terms of individualization of SWCNTs and low defect induced with the processing in the SWCNT walls is demonstrated by the long photoluminescence lifetimes and the elevated photoluminescence yield measured especially for PF12-wrapped SWCNTs. Further evidence of the exceptional quality of the samples is demonstrated by the high mobility and on/off ratio of the network field effect transistors fabricated with the PF12-wrapped SWCNTs. Hole and electron mobilities higher than 14 cm^2 V^{-1} s^{-1} are obtained for SO SWCNTs network field effect transistors with ion-gel gating.

Experimental Section

Materials: Large diameter (about 1.4 nm), high purity SWCNTs processed by arc plasma jet (SO) were purchased from Meijo Nano Carbon Co., Ltd. High-pressure carbon monoxide (HiPco) SWCNTs (diameter about 1.0 nm) was acquired from Unidym. Poly(9,9-di-*n*-octylfluorene-2,7-diyl) (PF8) was purchased from American Dye Source Inc.. All SWCNTs and PF8 were used as received without any treatments. Poly(9,9-di-*n*-hexylfluorene-2,7-diyl) (PF6), poly(9,9-di-*n*-dodecylfluorene-2,7-diyl) (PF12), poly(9,9-di-*n*-pentadecylfluorene-2,7-diyl) (PF15) and

© 2013 WILEY-VCH Verlag GmbH & Co. KGaA, Weinheim

poly(9,9-di-*n*-octadecylfluorene-2,7-diyl) (PF18) were synthetized for this study.

Synthesis of polymers: All polyfluorenes, except the PF8, were synthesized in a Yamamoto-type homocoupling reaction. A 20 mL microwave tube was charged with the 2,7-dibromo-9,9-dialkylfluorene (500 mg, 0.91 mmol). In a glovebox, bis(cyclooctadiene)nickel(0) (702 mg, 2.55 mmol) and 2,2'-bipyridyl (370 mg, 2.37 mmol) were added and the tube sealed under argon. 1,5-Cyclooctadiene (0.29 mL, 2.37 mmol) and dry THF (15 mL) were introduced via a syringe. Afterwards the reaction mixture was irradiated with microwaves (400 W) for 15 min to 120 °C. After completion of the reaction, the mixture was diluted with chloroform and subsequently extracted with 2 N aqueous HCl, concentrated aqueous $NaHCO_3$ solution, concentrated aqueous titriplex solution and brine. The solvent was removed by rotary evaporation. Afterwards, the residue was re-dissolved in chloroform and precipitated into cold methanol, followed by Soxhlet extraction with methanol, acetone, ethylacetate, and chloroform. The chloroform fraction was concentrated and re-precipitated into methanol to obtain the polyfluorene as a slightly yellow solid.

Molecular weight data: The molecular weights of polyfluorenes were determined by gel permeation chromatography (GPC). The measurements were carried out on a PSS/Agilent SECurity GPC System equipped with polystyrene gel columns (PSS SDV analytical linear M 8 × 300 mm, particle size 5 µm), and connected to an diode array detector (ALS G1329A) and an RI detector (RID G1362A), using THF as eluent.

PF6 M_n = 320 000, M_w = 850 000, PDI = 2.60; PF12: M_n = 34 200, M_w = 67 300, PDI = 1.97; PF15: M_n = 351 000, M_w = 1 080 000, PDI = 3.08; PF18: M_n = 336 000, M_w = 840 000, PDI = 2.50. The 2,7-dibromo-9,9-dialkylfluorene monomers were synthesized according to a procedure described in the literature.[31]

Dispersion of SWCNTs: For all SWCNT dispersions, 1 mg of sooth and 3 mg of polymer were added to 10 mL of toluene. The mixture was sonicated for 2 h in the cup horn of a high power sonicator (Misonix 3000) used at 90 W, during sonication the temperature of the sample was kept constant at 12 °C. Immediately after sonication, the dispersion was centrifuged at 16 000*g* for 2 h (Eppendorf centrifuge 5418) for the samples used for optical measurements and for several hours (with one step at 195 000*g* and a second step at 368 000*g*) with a Beckman Coulter (Optima XE-90; rotor: SW55Ti) for samples used to fabricate field effect transistors. The upper supernatant was taken and used for further measurements. For device fabrications, the pellet was taken and redispersed in 1 mL toluene.

Optical absorption spectroscopy: Absorbance spectra of the samples were recorded in a wavelength range from 300 to 2300 nm. A 2 mm and 1 cm path length quartz cells were used for samples with large diameter and small diameter SWCNTs, respectively. All measurements were done at room temperature using an UV-Vis-NIR spectrophotometer (Jasco V-570). The nanotube indexes are determined as described in the text following Equation 1, taking in account the medium used for the suspension. For the water-based suspension the attribution was not done, shifts respect to the toluene sample are expected due to the different dielectric constant ($\varepsilon_{r.toluene}$ = 2.4; $\varepsilon_{r.H2O}$ = 80.1).

Photoluminescence measurements: Steady state photoluminescence spectroscopy was carried out by exciting the sample at approximately 770 nm with a Ti:Sapphire laser operated in mode-locking. The duration of the pulses is about 150 fs and the repetition frequency ~76 MHz. The average excitation power was set to 2.0 mW for steady state measurements and 15 mW for the time resolved spectroscopy. The steady state photoluminescence was recorded with an InGaAs detector (Andor technology). The time resolved traces were recorded with a streak camera (Hamamatsu Photonics) with a NIR sensitive cathode working in synchroscan (time resolution about 2 ps). All measurements were performed at room temperature.

AFM microscopy: For AFM sample preparation, mica substrates were treated with nickel ion solution and then the SWCNT dispersion was deposited onto the treated surface. Finally, a stream of N_2 gas was used to dry the sample. AFM images were taken with a Bruker microscope (MultiMode 8 with ScanAsyst) in tapping mode with SNL-10 probes with elastic constant k = 0.58 N·m^{-1} and resonance frequency f = 40–75 kHz. The images were taken with a scan rate of 0.6 Hz and 1024 sample/lines.

Molecular Modelling: Nanotube structures were generated through Nanotube Modeler software.[32] Nanotubes are varied in length from 100 to 300 Å, open at both ends, and polyfluorenes contained from 16 to 20 repeat units. The hybrid structures composed of nanotubes and polyfluorenes were optimized by a sequence of 10 cycles of Impulse Dynamics in the microcanonical ensemble (T = 300 K, time step of 1 fs, selected atomic velocities of 1 Å·ps^{-1}) followed by energy minimizations. Dynamics cycles lasted for 5000 steps. By this technique, the initial atomic velocities are chosen according to Maxwell-Boltzmann distribution at a given temperature except for some selected part (polyfluorene chains in our simulations), which is assigned an initial velocity in the direction of the tube axis in the first cycle. The hybrids were built by adding polymer chains one by one -typically three polymer chains cover the entire nanotube surface, but more chains were added when needed. Calculations were carried out within CERIUS^2 computational package[33] using the CVFF950 force field.[34]

Transistor fabrication and characterization: The SWCNT dispersion was drop-cast on a thermally grown SiO_2 layer (230 nm thickness), on heavily doped Si wafer, following a previously reported method.[25] Two droplets of SWCNT dispersion (2 µl per droplet) were used for the channel formation of all devices. The droplets smeared to cover an area of approximately 7.1 mm^2. Interdigitated pattern of 30 nm Au with 10 nm Ti adhesive layer deposited on top of the SiO_2/Si wafer were used as source and drain electrodes. The transistor channel was 20 µm long. Prior to the SWCNT dropcasting, the substrates were functionalized by using self-assembled monolayer of 3-aminopropyl-triethoxysilane (APTES). The SWCNT transistor was vacuum annealed (5 × 10^{-2} mbar, 400 °C) for about 3 h. Ion gel of 1-ethyl-3-methylimidazolium bis(trifluoromethylsulfonyl)imide ([EMIM][TFSI])[26] was cast on the transistor channel and Pt foil was attached to form an ion-gel-gated transistor. The electronic transport characteristics of the SWCNT transistors were measured using an Agilent E5270B semiconductor parameter analyzer. The speed of voltage sweep for the measurement of ion gel transistors was 10 mV·s^{-1}. All steps for device fabrication and measurement were performed inside a dry nitrogen glovebox. The capacitance of the ion-gel gated SWCNT transistors was measured using an electrochemical impedance analyzer (Bio Logic, SP-200) with the used parameters reflected the conditions of transistor operations.

Acknowledgements

The collaborative research program between the University of Groningen and Wuppertal University was made possible with financial support by Stichting voor Technische Wetenschappen (STW, Utrecht, the Netherlands) and the Deutsche Forschungsgemeinschaft (DFG, Bonn, Germany). The European commission through the Erasmus Mundus Program EuroTango supported the stay in Groningen of G.D.C. E.J.F.C. acknowledges hospitality of Prof. S.J. Marrink's group at U. Groningen and the financial support from CAPES. M.C.S. thanks financial support from FAPESP.

Received: January 17, 2013
Revised: March 20, 2013
Published online: April 25, 2013

[1] R. Van Noorden, *Nature* **2011**, *469*, 14–16.
[2] R. Martel, T. Schmidt, H. R. Shea, T. Hertel, P. Avouris, *Appl. Phys. Lett.* **1998**, *73*, 2447–2449.
[3] P. Avouris, Z. Chen, V. Perebeinos, *Nat. Nanotechnol.* **2007**, *2*, 605–615.
[4] J. A. Misewich, R. Martel, P. Avouris, J. C. Tsang, S. Heinze, J. Tersoff, *Science* **2003**, *300*, 783–786.

© 2013 WILEY-VCH Verlag GmbH & Co. KGaA, Weinheim

[5] K. Jensen, J. Weldon, H. Garcia, A. Zettl, *Nano Lett.* **2007**, *7*, 3508–3511.
[6] G. A. Steele, A. K. Hüttel, B. Witkamp, M. Poot, H. B. Meerwaldt, L. P. Kouwenhoven, H. S. J. van der Zant, *Science* **2009**, *325*, 1103–1107.
[7] R. Martel, *ACS Nano* **2008**, *2*, 2195–2199.
[8] M. C. Hersam, *Nat. Nanotechnol.* **2008**, *3*, 387–394.
[9] M. S. Arnold, A. A. Green, J. F. Hulvat, S. I. Stupp, M. C. Hersam, *Nat. Nanotechnol.* **2006**, *1*, 60–65.
[10] S. Ghosh, S. M. Bachilo, R. B. Weisman, *Nat. Nanotechnol.* **2010**, *5*, 443–450.
[11] X. Tu, S. Manohar, A. Jagota, M. Zheng, *Nature* **2009**, *460*, 250–253.
[12] H. Liu, D. Nishide, T. Tanaka, H. Kataura, *Nat. Commun.* **2011**, *2*, 309.
[13] A. Nish, J.-Y. Hwang, J. Doig, R. J. Nicholas, *Nat. Nanotechnol.* **2007**, *2*, 640–646.
[14] J.-Y. Hwang, A. Nish, J. Doig, S. Douven, C.-W. Chen, L.-C. Chen, R. J. Nicholas, *J. Am. Chem. Soc.* **2008**, *130*, 3543–3553.
[15] M. Tange, T. Okazaki, S. Iijima, *J. Am. Chem. Soc.* **2011**, *133*, 11908–11911.
[16] H. Ozawa, N. Ide, T. Fujigaya, Y. Niidome, N. Nakashima, *Chem. Lett.* **2011**, *40*, 239–241.
[17] H. W. Lee, Y. Yoon, S. Park, J. H. Oh, S. Hong, L. S. Liyanage, H. Wang, S. Morishita, N. Patil, Y. J. Park, J. J. Park, A. Spakowitz, G. Galli, F. Gygi, P. H.-S. Wong, J. B.-H. Tok, J. M. Kim, Z. Bao, *Nat. Commun.* **2011**, *2*, 541.
[18] C. Blum, N. Stürzl, F. Hennrich, S. Lebedkin, S. Heeg, H. Dumlich, S. Reich, M. M. Kappes, *ACS Nano* **2011**, *5*, 2847–2854.
[19] F. Lemasson, N. Berton, J. Tittmann, F. Hennrich, M. M. Kappes, M. Mayor, *Macromolecules* **2012**, *45*, 713–722.
[20] M. Kwak, J. Gao, D. K. Prusty, A. J. Musser, V. A. Markov, N. Tombros, M. C. A. Stuart, W. R. Browne, E. J. Boekema, G. ten Brinke, H. T. Jonkman, B. J. van Wees, M. A. Loi, A. Herrmann, *Angew. Chem., Int. Ed.* **2011**, *50*, 3206–3210.
[21] J. Gao, M. A. Loi, E. J. F. de Carvalho, M. C. dos Santos, *ACS Nano* **2011**, *5*, 3993–3999.
[22] J. H. Choi, M. S. Strano, *Appl. Phys. Lett.* **2007**, *90*, 223114.
[23] D. W. Bright, F. B. Dias, F. Galbrecht, U. Scherf, A. P. Monkman, *Adv. Funct. Mater.* **2009**, *19*, 67–73.
[24] M. L. Connolly, *J. Appl. Cryst.* **1983**, *16*, 548–558.
[25] S. Z. Bisri, J. Gao, V. Derenskyi, W. Gomulya, I. Iezhokin, P. Gordiichuk, A. Herrmann, M. A. Loi, *Adv. Mater.* **2012**, *24*, 6147–6152.
[26] M. S. Kang, J. Lee, D. J. Norris, C. D. Frisbie, *Nano Lett.* **2009**, *9*, 3848–3852.
[27] H.T. Yuan, H. Shimotani, A. Tsukazaki, A. Ohtomo, M. Kawasaki, Y. Iwasa, *Adv. Funct. Mater.* **2009**, *19*, 1046–1053
[28] G. P. Siddons, D. Merchin, J. H. Back, J. K. Jeong, M. Shim, *Nano Lett.* **2004**, *4*, 927–931.
[29] S. M. Sze, K. K. Ng, *Physics of Semiconductor Devices*, John Wiley And Sons, **2007**.
[30] S. Ilani, L. a. K. Donev, M. Kindermann, P. L. McEuen, *Nat. Phys.* **2006**, *2*, 687–691.
[31] M. Grell, W. Knoll, D. Lupo, A. Meisel, T. Miteva, D. Neher, H.-G. Nothofer, U. Scherf, A. Yasuda, *Adv. Mater.* **1999**, *11*, 671–675.
[32] Nanotube Modeler version 1.6.4, J. Crystal. Soft., www.jcrystalsoft.com.
[33] Cerius2, version 4.10; Accelrys, Inc: San Diego, CA (2005).
[34] P. Dauber-Osguthorpe, V. A. Roberts, D. J. Osguthorpe, J. Wolff, M. Genest, A. T. Hagler, *Proteins* **1988**, *4*, 31–47.

© 2013 WILEY-VCH Verlag GmbH & Co. KGaA, Weinheim